HHS Public Access

Author manuscript

Acta Biomater. Author manuscript; available in PMC 2025 January 01.

Published in final edited form as:

Acta Biomater. 2024 January 01; 173: 135–147. doi:10.1016/j.actbio.2023.11.013.

Direct measurements of collagen fiber recruitment in the posterior pole of the eye

Po-Yi Lee[1,2], **Gosia Fryc**[3], **John Gnalian**[1], **Bingrui Wang**[1], **Yi Hua**[1,4,5], **Susannah Waxman**[1], **Fuqiang Zhong**[1], **Bin Yang**[6], **Ian A Sigal**[1,2,*]

[1]Department of Ophthalmology, University of Pittsburgh School of Medicine

[2]Department of Bioengineering, Swanson School of Engineering

[3]Department of Chemistry, Dietrich School of Arts and Sciences University of Pittsburgh, Pittsburgh, PA

[4]Department of Biomedical Engineering, University of Mississippi, University, MS

[5]Department of Mechanical Engineering, University of Mississippi, University, MS

[6]Department of Engineering, Rangos School of Health Sciences, Duquesne University, Pittsburgh, PA

Abstract

Collagen is the main load-bearing component of the peripapillary sclera (PPS) and lamina cribrosa (LC) in the eye. Whilst it has been shown that uncrimping and recruitment of the PPS and LC collagen fibers underlies the macro-scale nonlinear stiffening of both tissues with increased intraocular pressure (IOP), the uncrimping and recruitment as a function of local stretch have not been directly measured. This knowledge is crucial to understanding their functions in bearing loads and maintaining tissue integrity. In this project we measured local stretch-induced collagen fiber bundle uncrimping and recruitment curves of the PPS and LC. Thin coronal samples of PPS and LC of sheep eyes were mounted and stretched biaxially quasi-statically using a custom system. At each step, we imaged the PPS and LC with instant polarized light microscopy and quantified pixel-level (1.5 μm/pixel) collagen fiber orientations. We used digital image correlation to measure the local stretch and quantified collagen crimp by the circular standard deviation of fiber orientations, or *waviness*. Local stretch-recruitment curves of PPS and LC approximated sigmoid functions. PPS recruited more fibers than the LC at the low levels of stretch. At 10% stretch the curves crossed with 75% bundles recruited. The PPS had higher uncrimping rate and waviness remaining after recruitment than the LC: 0.9° vs. 0.6° and 3.1° vs. 2.7°. Altogether our

[*]**Correspondence:** Ian A. Sigal, Ph.D., Laboratory of Ocular Biomechanics, Department of Ophthalmology, University of Pittsburgh Medical Center, 1622 Locust St. RM 7.382, Pittsburgh, PA, USA. 15219, ian@OcularBiomechanics.com, www.OcularBiomechanics.com.

Disclosures: Fuqiang Zhong was at the University of Pittsburgh when he contributed to this work. Other authors have nothing to disclose.

findings support describing fiber recruitment of both PPS and LC with sigmoid curves, with the PPS recruiting faster and at lower stretch than the LC, consistent with a stiffer tissue.

Graphical Abstract

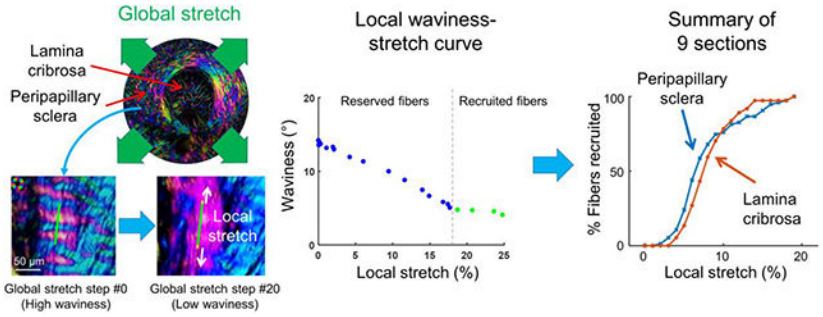

Keywords

recruitment; collagen; crimp; posterior pole; polarized light microscopy

1. Introduction

Collagen is the main load-bearing component of the sclera and lamina cribrosa (LC) in the posterior pole of the eye (Figure 1). [1–5] Collagen thus plays a critical role in how these tissues protect the delicate neural tissues of the retina and optic nerve and maintain the globe shape necessary for vision. [6, 7] The collagen fibers of both sclera and LC exhibit the process known as fiber recruitment, [8, 9] giving rise to their well-known macro-scale nonlinear behavior (Figure 2). [10–14] While fiber recruitment as a function of intraocular pressure (IOP) has been measured, [14] no studies have directly measured the uncrimping and recruitment of the collagen fibers of the LC and adjacent peripapillary sclera (PPS) as a function of stretch. This knowledge is crucial to developing constitutive models of the tissues associating the micro and macro scales, which must be constructed based on the tissue stretch and not IOP. [15, 16] The knowledge is also necessary to understand the role of collagen fiber characteristics in the physiology and pathophysiology of the region. Because of the complex architecture and mechanical interactions between the PPS and LC, it is not trivial to infer recruitment as a function of stretch from recruitment as a function of IOP.

Our goal in this study was to characterize the stretch-induced collagen fiber uncrimping and recruitment of the LC and adjacent PPS at the fiber level. We hypothesized that collagen recruitment in the PPS occurs at lower levels of stretch than in the LC. This suspicion is based on three elements: First, previous studies have consistently found, or argued rationally, that the LC is more compliant than the sclera, with estimates suggesting a difference of about an order of magnitude. [10, 16–21] One potential mechanism underlying the differences in compliance could be if the fibers in the LC recruit at higher levels of stretch than the fibers in the PPS. Second, experimental evidence has demonstrated that the PPS surface suffers only low single digits of stretch (maximum principal strain) even for a large IOP increase from 5 to 45 mm Hg. [2, 22]. To provide context, normal IOP ranges

from 11 to 21mmHg, [23] such that the expected PPS deformations within the normal and near-normal IOP range are likely even smaller. For the PPS deformations to be this small strongly suggests that PPS fibers also recruit at low single digits of stretch. If this was not the case, it seems reasonable to expect that the tissues would remain highly compliant and thus exhibit larger deformations. Third, in our measurements of LC and PPS uncrimping as a function of IOP, we found that the fibers of the sclera recruited at lower levels of IOP than those of the LC. [14] Those measurements were obtained using inflation testing of whole globes, maintaining tissue integrity and preserving the interactions between the PPS and LC. This means that the behavior of one tissue can affect that of the other. Many studies have shown that the mechanical properties of the sclera play a much larger role in the mechanical response of the ONH to changes in IOP than the properties of the LC. [24, 25] Moreover, the studies show that variations on sclera properties have very large and direct effects on the response of the LC to IOP, whereas variations of LC properties have trivial effects on the response of the PPS to IOP. This has generally been attributed to the fact that the LC is much smaller than the sclera surrounding it. For context, a normal human LC has a volume of 0.49 to 1.15 μl with a thickness ranging between 142 and 272 μm. The PPS with a thickness that can reach 1200 μm can have a volume 50 times larger than that of the LC within a few mm of the scleral canal. [26] We should note that the actual effects of a stiffer/compliant sclera on the LC are actually quite complicated due to the interactions of multiple factors. [27, 28] While inflation testing has the advantage of being physiologically realistic, IOP is not a suitable parameter to determine how the tissues behave independently, which is also of interest. Based on these, we suspected that the LC and PPS recruitment curves may be more similar when plotted as a function of IOP, when the tissues interact, than as a function of strain, when the tissues are independent. Testing this prediction is one of the motivations for this work. By evaluating the recruitment as a function of local stretch instead of IOP, in this study, we were able to measure directly stretch-induced fiber responses of PPS and LC and remove any potential effects from interactions with other tissues. To achieve our goals, we used a recently introduced technique, instant polarized light microscopy (IPOL), which allows measuring directly and with high accuracy the stretch-induced uncrimping at the fiber-scale without the need for labels or stains.

2. Methods

A note on terminology:

Ocular collagen has a complex hierarchical organization. [29–34] In some regions, such as the cornea, the hierarchy is relatively well characterized, with collagen organized into evenly-spaced micro-fibrils approximately 35nm in diameter that join to form fibrils, then fibers, then lamellae. [33, 35–37] Collagen in the PPS and LC is more complex and not nearly as well understood. The analysis in this work is based on biaxial stretch testing (Figure 3) as well as visualizing and measuring collagen features at the micro-scale revealed by IPOL (Figures 4 and 5). It is at this scale that the undulations and crimp we refer to have been reported and measured. It is at this scale that the undulations and crimp we refer to have been reported and measured. [14, 31] While the images show what look like fibers, like those in the cornea, we expect these to have a sub-structure. To acknowledge this important

fact, we decided to refer to them as “fiber bundles”. In the hierarchical structure it is likely that these fiber bundles group into larger bundles.

Sample Preparation

Three eyes from one-year-old sheep were obtained from a local abattoir and processed within four hours after death as described elsewhere. [38] Briefly, the muscles, fat, and episcleral tissues were carefully removed. The optic nerve head (ONH) region was isolated using an 11-mm-diameter trephine and embedded in optimum cutting temperature compound (Tissue-Plus; Fisher Healthcare, TX, USA). Samples were then snap frozen in liquid nitrogen-cooled isopentane and sectioned coronally at a thickness of 16 μm. The samples were then washed with PBS to remove cutting compound. The tissues were never fixed or labeled. To ensure robust analysis we made sure to have three good sections for each eye (no breaks, folds or other artifacts), *i.e.*, 9 sections from 3 sheep eyes were used and analyzed in total.

Biaxial Stretch Testing

Each tissue section was mounted on a custom biaxial micro-stretcher system following previously reported methodology. [38] Briefly, two pieces of silicone sheeting (Medical Grade, 0.005”; BioPlexus, AZ, USA) were used to sandwich the tissue section to prevent curling or tears at the clamp points and to keep the tissue section fully hydrated. Only at the clamps was the silicone in tight contact with the tissue. The section was stretched equally along two orthogonal axes, quasi-statically followed by long (20s or more) pauses to allow dissipating viscoelastic effects in 0.5 mm stretch steps. We refer to the clamp-to-clamp stretch as global stretch (Figure 3).

Imaging

Each section was imaged using IPOL following previously reported methodology to visualize the collagen. [39] IPOL allows label-free visualization and quantification of collagen structure and orientation via color information for each pixel. Briefly, a set of polarization encoder and decoder were retrofitted into a brightfield microscope, where one consisted of a polarizer and a clockwise polarization rotator and the other consisted of an analyzer and a counter-clockwise polarization rotator. A region with low or no birefringence appeared dark since the polarizations of the white light had no change and thus was blocked. A birefringent sample, such as collagen, appeared colorful since IPOL differentiated the polarizations with wavelengths and thus changed the spectrum of the white light. The colorful light was acquired by a color camera to produce the true-color images indicating collagen fiber orientation. [40]

IPOL was implemented with a commercial inverted microscope (IX83; Olympus, Tokyo, Japan), a color camera (DP74, Olympus, Tokyo), and a 4x strain-free objective (numerical aperture 0.13, 1.5 μm/pixel). At each stretch step, multiple images were captured to cover the entire ONH region in a mosaic. Images with 20% overlap were acquired using a translational stage and stitched into mosaics using Fiji. [41] We have shown that the visualization of collagen fibers is not affected by mosaics or stitching. [31, 42] Autofocus was applied to avoid out-of-focus images during the stretch.

Collagen Crimp Quantification

IPOL is based on the optical properties of the collagen molecules, and therefore it allows accurate quantification of collagen orientation without the need to resolve and distinguish fibrils, fibers, or bundles. Pixel-scale collagen fiber orientations were determined by matching hue values over a pre-calibrated color-angle conversion map for corresponding angles. [38] In IPOL images, the hue values indicate the local orientation. Hence, straight fibers can be recognized because they have a constant color. Conversely, undulating fibers vary in orientation and thus in color. Regular color stripes are convenient to discern crimp from a visual, qualitative, perspective (Figure 4 left). As the tissue is stretched, the color stripes disappear and are replaced by more uniform coloring, this indicates fewer undulating fibers with decreased crimp (Figure 4 right). The objective analysis of crimp and of stretch-induced changes in crimp required careful quantification, as described in the following paragraph.

A custom MATLAB program was developed for manually placing rotatable rectangular regions on PPS and LC along crimp directions. As a measure of crimp, we computed "waviness" defined as the circular standard deviation of the pixel-level fiber angles within the rectangular region. The circular standard deviation (S) is defined as

$$S = \sqrt{-2\ln(R)}$$

where R is the mean resultant length of the data, defined as

$$R = \left| \frac{1}{N} \sum_{j=1}^{N} e^{i \cdot \theta_j} \right|$$

where N is the number of angle values and θ is the angle value.

For wavy crimped fiber bundles, the orientation distribution was bimodal and wide, indicated by higher waviness values (Figure 5 left). For straight, or recruited, fiber bundles, the distribution was unimodal and narrow, indicated by smaller waviness values (Figure 5 right). We tracked the long axis of the rectangular region using digital image correlation and then updated the region based on the elongation and displacement of the long axis from the tracking result at each step [43]. An evaluation of the accuracy of tracking results is shown in Supplementary Figure 1. We then measured the waviness in the updated rectangular region at each global stretch step until tissue failure. Local stretch was calculated by the length change in the long axis of the rectangular region (Figure 3). From the waviness-stretch data, we determined if a fiber bundle was recruited when the waviness no longer decreased with stretch, and then measured "% stretch to recruit" and "waviness when recruited" of recruited fiber bundles. We then used linear regression on the waviness-stretch data before recruitment to obtain the "uncrimping rate" as the absolute magnitude of the slope k (Figure 6). The rationale and implications of the definition of fiber recruitment and the waviness when recruited measurement are addressed in the Discussion. Note that we observed that some PPS and LC fiber bundles did not recruit with the stretch. We suspect that this was in cases where tissue processing had broken the fibers, disconnecting them

from one another and/or the matrix. In the local stretch analysis, we focused on the collagen fiber bundles that did recruit.

Statistical analysis

Linear mixed effect models accounting for correlations between measurements from the same sections and eyes were used to analyze the differences in waviness between the PPS and LC at each stretch step, and the differences in waviness when recruited and uncrimping rate between the PPS and LC. Descriptive statistical calculations such as angular mean and standard deviation were made using circular statistics. [4, 44] All statistical analyses were done using R. [45]

3. Results

We obtained the percentages of fiber bundles recruited at given local stretch in the LC and PPS (Figure 7a). In the recruited fiber bundles, we found that the uncrimping rate in the PPS (0.9±0.5) was significantly higher than that in the LC (0.6±0.3) (P's < 0.001) (Figure 7b). We found that the PPS recruited waviness when recruited (3.1°±0.9°) was significantly higher than the LC waviness when recruited (2.7°±0.7°) (P's < 0.05) (Figure 7c).

Waviness of both PPS and LC decreased with global stretch (Figure 8). At the initial state, the waviness was significantly higher in the PPS (10.4°±2.7°) than in the LC (8.3°±2.6°) (P's < 0.001). The difference was no longer significant between PPS (3.5°±1.2°) and LC (3.3°±1.2°) after the tissues were stretched (P's < 0.001).

4. Discussion

We applied image-based stretch testing to measure local stretch-induced collagen fiber bundle uncrimping and recruitment of the PPS and LC. Three main results arise from this work. First, PPS fiber bundles recruit at lower levels of local stretch than LC fiber bundles but both tissue recruitment curves were similar. Second, PPS fiber bundles had a higher uncrimping rate than LC fiber bundles. Third, waviness when recruited in the PPS and LC were non-zero. Below we discuss each of these in turn.

PPS fiber bundles recruit at lower levels of the local stretch than LC fiber bundles but both tissue recruitment curves were similar.

Only recruited fibers bear substantial loads, [14, 31, 46–48] and therefore the local stretch-recruitment curves reveal key information on the relative fraction of potentially load-bearing fiber bundles that are actually bearing the load. The results in this work reveal that a larger fraction of PPS fiber bundles bear the load when the stretch is small (<10%), a difference in the rate of regional stiffening under stretch. This is consistent with the general impression in the literature that the LC is more compliant than the sclera. [10, 16–21] This supports the concept that PPS stiffening at a lower level of stretch could be a protective mechanism that allows the PPS to resist large deformations at low and moderate IOPs, relieving the LC loads and protecting the fragile nerve fibers in the LC from vision-threatening insult.

The phenomenon that recruitment implies that not all fibers are always contributing to bear loads is well understood in other soft tissues, like tendon and ligament. [49, 50] A comparison of the collagen fiber recruitment curves versus stretch for the PPS and LC with other soft tissues is shown in Figure 9. Interestingly, whilst all curves roughly follow the sigmoid shape observed in this work, the curves vary widely in the starting points and steepness. The recruitment curves of the PPS and LC are situated within the region between the curves of the rat tail tendon and rat bladder. While the findings support the hypothesis that collagen recruitment in the PPS occurs at lower levels of stretch than in the LC, in the context of many tissues, the differences we observed between PPS and LC appear rather small. On this we venture to speculate that this could occur if these two tissues have adapted to exhibit a similar range of responses under load, ostensibly to better protect the neural tissues within the canal. Some studies have suggested that very different responses between PPS and LC could cause concentrations of stress or strain that could adversely affect the neural tissues. [5] More work is required to determine if this speculation stands.

While the findings support our hypothesis that collagen recruitment in the PPS occurs at lower levels of stretch than in the LC, we were surprised by the similarity between the recruitment curves for both tissues. Similar curves indicate similar rates of PPS and LC stiffening under stretch. We recently conducted a study in which we used computational modeling to estimate recruitment curves as a function of IOP in seven regions of the corneoscleral shell. [51] As expected, all regions exhibited sigmoid curves, but the recruitment rates varied substantially over the globe. We found that the fibers of the posterior equator recruited the fastest at low IOPs, such that at 15mmHg over 90% of the fibers were recruited. The fibers of the PPS recruited much slower with IOP, such that only 34% of the PPS fibers were recruited at a physiologic IOP of 15 mmHg. At an elevated IOP of 50mmHg, 70% of the PPS fibers had been recruited. Experimental studies of IOP-induced sclera deformation have shown that even at elevated IOPs, the PPS undergoes single-digit levels of stretch. [11, 52, 53] Together, those results are consistent with this work in that we measured 75% recruitment in PPS at 10% local stretch.

The recruitment curves for PPS and LC cross at 10% stretch, with both tissues exhibiting 75% recruitment. It is interesting to compare this finding with those in a recent study in which we analyzed crimp in the LC and PPS. [14] The study was similar to this one, but with two important differences: we measured crimp as a function of IOP, not as a function of stretch as in this work. The study was cross-sectional, using samples fixed at specific IOPs. Despite the differences, the results from both studies are remarkably consistent with one another. In the previous study, the recruitment curves of the PPS and LC were similar, as in this work, with the PPS exhibiting higher recruitment at IOPs under 15mmHg. Interestingly, both curves crossed at a physiologic IOP of 15mmHg, with 75% of collagen fibers recruited in both PPS and LC. The recruitment curves are slightly different at higher IOPs or higher levels of stretch, although both studies coincide in that there was substantial collagen waviness in both the PPS and LC even at very high IOPs.

An important consideration when interpreting our findings is that the recruitment curve is only related to the rate of stretch-induced stiffening, which may be very different from the actual tissue stiffness. The results above should not be interpreted as indicative of which

tissue is stiffer. In addition to the crimp angle, a computational modeling approach [48] has shown that the elastic modulus of the filament E and the ratio of the amplitude of the helix to the radius of the filament cross-section R_0/r_0 affect the stretch-dependent stiffening of collagen. Interestingly, Grytz and colleagues found that, everything else being equal, the initial crimp angle has almost no influence on the overall shape of the stress and stiffness function. In a later study, Grytz and colleagues used computational modeling to infer micro-scale fiber crimp and mechanics from macro-scale experimental data on posterior pole inflation.[11] They found that collagen fibril strain and recruitment rate were similar between the peripapillary and the mid-peripheral regions at the micro-scale, but the in-plane strains were significantly higher in the peripapillary region than in the mid-periphery.

In this study, we considered tissues as part of the LC or PPS, without further details of their location within the ONH. In an earlier cross-sectional study we analyzed the collagen crimp in eyes fixed at 0, 5 or, 10mmHg IOP. [9] Crimp was characterized by period, not waviness as in this work. Elsewhere we have discussed the relationship between these two measures. [14, 31] In a previous study, we found that the crimp periods were smaller and less variable in the LC than in the PPS. The crimp period in the PPS increased with distance from the canal. [9] We interpreted those findings as indicative that the tissues of the ONH are adapted to prevent very different deformations at the scleral canal edge region that could insult the neural tissues. This is consistent with our findings in this work that the waviness was smaller in the LC than in the PPS. We note that this did not have to be the case because crimp period and waviness are distinct measures of crimp and can vary independently. This has been discussed in detail elsewhere. [14, 31]

PPS fiber bundles had a higher uncrimping rate than LC fiber bundles.

Uncrimping rate is closely associated with the shape of the crimp. [54] Physically-based structural models have been developed to describe how the configuration of collagen evolves under load and predict the non-linear mechanical behavior of collagen fiber microstructures that undergo large deformations. [33, 54–58] Collagen crimp can be viewed as an extensible helical spring, i.e., a rod wound around the central axis of a cylinder with a radius R_0. [48, 59] In the structural model, a plane sinusoidal crimp [$R_0 = 0$] has a higher uncrimping rate than a helical crimp [$R_0 > 0$]. [54] PPS fiber bundles having a higher uncrimping rate is consistent with the collagen configuration of PPS being closer to a plane sinusoidal structure. In geometry, a plane sinusoidal structure allows for “packing” more collagen in a unit volume than a helical structure. This is supported by IPOL images (Figure 4) that the density of collagen in the PPS regions is higher since PPS regions in IPOL images are brighter than LC regions. Again, this is consistent with an LC that is more compliant than the PPS. [10, 16–21] It is worth noting that PPS fiber bundles had a higher uncrimping rate but the “% stretch to recruit” of PPS was lower at higher stretch. It is because the waviness of the collagen fibers in the PPS was larger and more variable than that of the LC at the initial and early stretching states (Figure 8). The high uncrimping rate led to the waviness of collagen fibers in the PPS being close to that of the LC after the tissues were stretched. However, even though the uncrimping rate was higher in the PPS, some PPS fiber bundles with high waviness still required more local stretch to achieve recruitment.

Waviness when recruited in the PPS and LC were non-zero.

Waviness when recruited relates to the ability of a fiber bundle to bear the load and resist being fully uncrimped under stretch. Ideal fiber recruitment happens when a fiber is fully straightened (*i.e.*, zero waviness). However, interactions between fibers may prevent the fibers from being fully straightened. For example, stretch cannot fully remove fiber twisting and bending and thus such fibers always present residual crimp under large stretch (Figure 10). High waviness when recruited thus could indicate a more complex fiber microstructure. Moreover, it is worth noting that an elevated load could potentially increase the waviness of these microstructures. The examples show only uniaxial loading, which is known to lead to fiber alignment with the load, through rotation, if possible, bending if not. The tissues of the PPS, and to some extent those of the LC, are subjected to biaxial loading. Studies using inflation have even suggested that at the macro-scale the sclera is sometimes close to an equi-biaxial stretch. [60] At the micro-scale, the situation is more complex. This could explain the findings from our previous study, where the recruitment percentages of PPS and LC decreased for IOP increases between 20 mmHg and 50 mmHg, as the recruitment was determined based on waviness thresholds in that study. [14] Such microstructure has been recognized in fibrillar-level tendon and ligament, which fulfill local fibril flexibility and behave as biological hinges both absorbing tension and guiding the recoil of collagen fibers. [61, 62] The interactions between fibers that result from the complex microstructure and interweaving can also have major effects at the tissue macro-scale. [3]

It is important to note that the relationship between waviness and local stretch measurements may be different from the relationship between waviness and global or macro-level stretch. Global stretch often results in varying local stretch, leading to also varying different levels of recruitment and stiffening between regions. Local stretch measurements allow tracking the continuous uncrimping process of an individual fiber bundle. These measurements exclude macro-level sample displacements and deformations during testing, such as unfolding, rotations, and slip.

In a previous study, we evaluated collagen fiber recruitment based on analyzing crimp differences using different samples fixed at specific IOPs. [14] Our previous and current studies are similar but with two important differences (Figure 10): previously we measured crimp as a function of IOP, not as a function of stretch as in this work. The study was cross-sectional, using samples fixed at specific IOPs. The IOP caused stretch in the PPS and LC region, resulting in fiber uncrimping. However, for each individual eye, the same IOP might induce different stretch levels due to different mechanical properties. Directly measuring the relationship between uncrimping and local stretch fills the gap between the IOP and uncrimping. In addition, tissues, including neural tissue and cells, are sensitive to the stretch instead of IOP. The stretch relates to tissue response and remodeling. Measuring the uncrimping and recruitment of collagen fibers as a function of local stretch helps develop accurate constitutive models that capture the mechanical behavior of collagenous tissues. Collagen fibers play a vital role in providing mechanical strength and stiffness to collagenous tissues. [32, 63] By understanding how collagen fibers respond to stretching, we can accurately represent the complex mechanical properties of these tissues. The uncrimping and recruitment of collagen fibers reveal important insights into the nonlinear stress-strain

relationship and anisotropic behavior of collagenous tissues. [3, 13, 14, 64, 65] These measurements help us understand how collagen fibers align and orient themselves under different levels of stretch, providing a foundation for capturing the anisotropic mechanical response of tissues. Moreover, monitoring the uncrimping and recruitment of collagen fibers allows us to study tissue remodeling processes that occur in response to mechanical loading. [17, 66–68] By incorporating this knowledge into constitutive models, we can improve our understanding of tissue behavior under physiological and pathological conditions, enhancing clinical applications and treatment strategies.

It is important to note that our current study differs from our previous work [14] in terms of methodology and focus. In our previous study, we analyzed crimp differences in fixed samples at specific IOPs, providing statistical behavior of the entire sample set. Nonetheless, this approach did not report the recruitment behavior at a specific beam or fiber bundle. In contrast, our current study overcomes these limitations by measuring the recruitment behavior of each individual fiber at various stretch levels, enabling us to establish the relationship between uncrimping and local stretch, such as the uncrimping rate and waviness when recruited of individual fiber bundles. This relationship reveals important aspects of the microstructure change of collagen during uncrimping, and can be further used for accurately capturing the mechanical behavior of collagen fibers in the development of constitutive models.

We should note that our goal in this work was not to introduce an innovative approach to test experimentally samples of PPS and LC. Our goal was to provide information, previously unavailable, through the systematic direct measurement of collagen fiber uncrimping and recruitment of the PPS and LC. Previous methods to indirectly measure collagen PPS and LC uncrimping were cross-sectional and have important limitations, as discussed extensively before. [14] Similarly, inverse models, [48] while powerful, are also not direct measurements. In this study, the ability to measure uncrimping processes with high angular resolutions afforded by instant polarized light microscopy (IPOL) and in the fragile and thin tissue region is a substantive step forward. Direct measurements allow identifying collagen crimp morphology when the individual fiber bundles recruit and the relationship between collagen crimp morphology and stretch. Among other potential applications, discussed later in this work, such information will help develop more accurate constitutive models to describe ocular tissue mechanics. [69–71] Direct measurements of stretch-induced change in crimp help understand the nonlinear mechanical behavior of the posterior pole and build the connection between tissue stiffness and aging/age-related diseases in the eye. [72–74]

In this study, we used a polarized light imaging technique, introduced in 2021, IPOL, to visualize collagen fiber orientation and microstructure via a color snapshot. [39] IPOL has high spatial and angular resolutions, making it uniquely well-suited to discern challenging aspects of the ONH collagen microarchitecture, such as crimp (Figure 5). This is particularly important for LC and PPS that have relatively small crimp, that cannot be measured well using tracing techniques that are common in vascular tissues. [46] Current versions of polarization sensitive optical coherence tomography [75] or wide-angle X-ray scattering [76] do not have sufficient spatial or angular resolution. MRI can discern PPS crimp, [77] but the complexity and cost of the system and the need to use a so-called magic angle technique

makes it impractical at this moment. Some studies have used imaging techniques with higher magnifications such as confocal and multiphoton imaging [78, 79], but these have much smaller fields of view, complicating analysis. Further, they often require substantial tissue processing. A crucial strength of IPOL for this work is that it does not require labels or stains, making the process simpler and avoiding steps that could affect tissue structure and/or mechanics. IPOL also has a high temporal resolution, limited only by the frame rate of the camera. Although we had to use IPOL with mosaicking to capture a wide region, the frame rate of IPOL was still faster than polarized light imaging techniques that require multiple polarization acquisition [42] and scanning-based imaging techniques such as second harmonic imaging. [80] For this particular work faster imaging was helpful to prevent tissue dehydration during stretch testing.

The definition of waviness is the same that we have used elsewhere. [4, 14, 31] This definition is convenient because it naturally results in a waviness measure that is bound at zero, for perfectly straight fibers where all the angles are identical. Waviness is only one possible measure of crimp. Elsewhere we, and others, have characterized crimp using period, amplitude, tortuosity, crimp angle, maximum deviation angles, and other measures. [4, 31, 46, 48, 54, 81] In many of these cases, it is possible to base on simplifying assumptions about the shape of the crimp, for example, that it is well described by a perfect helix, and to convert from one measure to another. An advantage of waviness as computed in this work is that it does not require assuming a particular shape for the collagen crimp, or to assume that it is regular. Given the complexity and variability of the collagen fiber undulations in the tissues studied, we saw this as an advantage, even though we acknowledge that it may not be trivial to compare with crimp data elsewhere reported with other measures.

There are multiple reasons to study collagen fiber waviness, or crimp, and of the effects of stretch other than the development of constitutive models. One reason is that a characterization of the waviness of the collagen fibers can provide insights into the mechanistic origins of the mechanical behavior of the tissue. [63, 82, 83] These insights include the origin of the tissue strength, elasticity, viscoelasticity, and other properties that constitutive models aim to capture but not necessarily explain or fully account for. [84, 85] Collagen waviness itself is the result of specific biochemical and biomechanical conditions. Fiber waviness, for instance, can both indicate and play a role in tissue growth and development, and/or of integration of transplanted or regenerated tissue. [85–87] Fiber waviness is affected by the type, distribution, activity, and other characteristics of the cells within tissues. Conversely, waviness or changes in waviness can affect the cells. As such, a good characterization of crimp may also help identify the roles of different components in tissue function, including but not limited to mechanics. Abnormal crimp could provide insight into the conditions at smaller scales that can be easily discerned with a microscope. [88, 89] Waviness can also be used as a way to sense or confirm local effects of load. For example, a lack of collagen fiber waviness in an arterial wall could be indicative of increased blood pressure. [89] Some aspects of collagenous tissue remodeling have been shown to be less dependent, and even independent, of the resident cell activity. [90] This can potentially underlie why some tissues or species regenerate better than others.

The work presented here is subject to several limitations. First, we conducted research on sheep eyes, which share with human eyes the crucial trait of having a collagenous LC. [91] Sheep eyes have been studied as a model of experimental ocular hypertension and glaucoma. [92, 93] Sheep eyes, however, also have some differences with human eyes, such as a ventral groove in the ONH. [94] How much this groove affects ONH biomechanics remains unclear, although it seems likely that ONH biomechanics of sheep eyes are much more similar to those of human eyes than those of mouse or rat and other common models. [95] Even if there are differences with the human ONH, understanding the eyes of sheep is important from a fundamental science perspective.

Second, our study was based on a section. Stretching tissue sections is a substantial simplification. It is crucial to acknowledge that this is not a condition intended to represent the physiological state. This setup is intended to help overcome the extremely challenging task of figuring out the mechanisms of collagen recruitment in posterior pole tissues of a whole sample. We contend that our setup is useful for micro-mechanical testing to understand tissue fundamental mechanics. By isolating the tissue section, we were able to visualize and analyze quantitatively in-plane fiber bundles. The signals of collagen fibers decrease with fiber inclination (*i.e.*, out-of-plane orientation). [96] Therefore, analyzing the bright regions allowed identifying the fibers primarily aligned in the section plane as well as the stretching plane. In this sense, we were able to visualize the fibers that are responding to the load. Measurement of collagen architecture and crimp in thick tissues is possible, but current methods are complex and do not have the spatial or angular resolution necessary. [97, 98]

Third, biaxial stretch testing is an approximation to simulate the effects of IOP or other loads. The global stretch is different from physiological loading. Although inflation experiments can be applied to whole eye globes and are more physiologic, currently it is not possible to track the uncrimping processes due to the limited imaging resolution and penetration. [97, 98] An alternative approach is to fix and section the tissues, but then the crimp can only be studied at one IOP. [14] Overall, our methods should be thought of as providing measurements that are realistic for the local micro-mechanical fiber behavior, such as local stretch-induced uncrimping, and not of the macro-scale or global behavior. There have been several studies in which the ONH and posterior pole biomechanics have been studied using a two-dimensional approximation [70, 99, 100] We posit that the loading applied to LC beams is likely more realistic than the loading applied to the PPS regions. That is because the neural tissues adjacent to the beams are substantially more compliant than the beam, allowing for bundle displacement and rotation, and thus the stretch is in-plane and along the beam.

Lastly, our setup did not provide any information on the forces through the tissue samples. It is essential to note that the focus of this investigation was the quantitative characterization of two important aspects of collagen fiber behavior: uncrimping and recruitment as a result of stretch. These two parameters are indicative of the microstructure and micromechanics of the tissue. We recognize that uncrimping and recruitment data can also be used to develop constitutive models of tissue biomechanics, and we believe that this should be possible. We note that there have been several excellent studies relating to ocular tissue microstructure

and mechanics, often including the development of constitutive models. [101–105] This, however, would require a different experimental setup than what we used. In addition, based on our images and the literature, we suspect that future constitutive models at the microscale level would benefit from incorporating other factors that can impact the forces and stresses, such as fiber-fiber interactions, cross-linking and hydration [3, 6, 91, 106–112] Unfortunately, these specific measurements were not available in the scope of our current study.

In conclusion, we quantified the changes in collagen waviness in the PPS and LC under local stretch. We derived tissue-specific recruitment curves and reported several parameters including waviness when recruited and uncrimping rate, which encode information on tissue microstructure and crimp types. We found that while the PPS fibers recruit at lower levels of stretch than the LC, the two tissues have similar recruitment curves. Both curves cross at about 10% stretch with 75% collagen fiber recruitment. Interestingly, in a previous cross-sectional study of recruitment as a function of IOP, we had found that curves for PPS and LC cross at normal IOP (15 mmHg) and 75% recruitment. Altogether, our findings have demonstrated that image-based stretch testing allows for characterizing microstructural collagen crimp properties of the posterior pole.

Supplementary Material

Refer to Web version on PubMed Central for supplementary material.

Funding:

Supported in part by National Institutes of Health R01-EY023966, R01-EY028662, P30-EY008098 and T32-EY017271 (Bethesda, MD), the Eye and Ear Foundation (Pittsburgh, PA), and Research to Prevent Blindness (unrestricted grant to UPMC ophthalmology, and Stein innovation award to Sigal IA).

References

1. Ethier CR, Johnson M, and Ruberti J, Ocular biomechanics and biotransport. Annual Review of Biomedical Engineering, 2004. 6: p. 249–273.
2. Coudrillier B, Tian J, Alexander S, Myers KM, Quigley HA, and Nguyen TD, Biomechanics of the human posterior sclera: age-and glaucoma-related changes measured using inflation testing. Investigative Ophthalmology & Visual Science, 2012. 53(4): p. 1714–1728. [PubMed: 22395883]
3. Wang B, Hua Y, Brazile BL, Yang B, and Sigal IA, Collagen fiber interweaving is central to sclera stiffness. Acta Biomaterialia, 2020. 113: p. 429–437. [PubMed: 32585309]
4. Gogola A, Jan N-J, Brazile B, Lam P, Lathrop KL, Chan KC, and Sigal IA, Spatial patterns and age-related changes of the collagen crimp in the human cornea and sclera. Investigative Ophthalmology & Visual Science, 2018. 59(7): p. 2987–2998. [PubMed: 30025116]
5. Midgett DE, Jefferys JL, Quigley HA, and Nguyen TD, The inflation response of the human lamina cribrosa and sclera: Analysis of deformation and interaction. Acta Biomaterialia, 2020. 106(1): p. 225–241. [PubMed: 32044458]
6. Hua Y, Voorhees AP, Jan N-J, Wang B, Waxman S, Schuman JS, and Sigal IA, Role of radially aligned scleral collagen fibers in optic nerve head biomechanics. Experimental Eye Research, 2020. 199: p. 108188. [PubMed: 32805265]
7. Huang W, Fan Q, Wang W, Zhou M, Laties AM, and Zhang X, Collagen: a potential factor involved in the pathogenesis of glaucoma. Medical Science Monitor Basic Research, 2013. 19: p. 237. [PubMed: 24002298]

8. Bailey AJ, Structure, function and ageing of the collagens of the eye. Eye, 1987. 1(2): p. 175–183. [PubMed: 3308525]

9. Jan N-J, Gomez C, Moed S, Voorhees AP, Schuman JS, Bilonick RA, and Sigal IA, Microstructural crimp of the lamina cribrosa and peripapillary sclera collagen fibers. Investigative Ophthalmology & Visual Science, 2017. 58(9): p. 3378–3388. [PubMed: 28687851]

10. Grytz R, Sigal IA, Ruberti JW, Meschke G, and Downs JC, Lamina cribrosa thickening in early glaucoma predicted by a microstructure motivated growth and remodeling approach. Mechanics of Materials, 2012. 44: p. 99–109. [PubMed: 22389541]

11. Grytz R, Fazio MA, Libertiaux V, Bruno L, Gardiner S, Girkin CA, and Downs JC, Age-and race-related differences in human scleral material properties. Investigative Ophthalmology & Visual Science, 2014. 55(12): p. 8163–8172. [PubMed: 25389203]

12. Liu X, Wang L, Ji J, Yao W, Wei W, Fan J, Joshi S, Li D, and Fan Y, A mechanical model of the cornea considering the crimping morphology of collagen fibrils. Investigative Ophthalmology & Visual Science, 2014. 55(4): p. 2739–2746. [PubMed: 24692124]

13. Geraghty B, Jones SW, Rama P, Akhtar R, and Elsheikh A, Age-related variations in the biomechanical properties of human sclera. Journal of the Mechanical Behavior of Biomedical Materials, 2012. 16: p. 181–191. [PubMed: 23182387]

14. Jan N-J and Sigal IA, Collagen fiber recruitment: a microstructural basis for the nonlinear response of the posterior pole of the eye to increases in intraocular pressure. Acta Biomaterialia, 2018. 72: p. 295–305. [PubMed: 29574185]

15. Girard MJ, Downs JC, Burgoyne CF, and Suh J-KF, Peripapillary and posterior scleral mechanics —part I: development of an anisotropic hyperelastic constitutive model. Journal of Biomechanical Engineering, 2009. 131(5): p. 051011. [PubMed: 19388781]

16. Grytz R, Meschke G, and Jonas JB, The collagen fibril architecture in the lamina cribrosa and peripapillary sclera predicted by a computational remodeling approach. Biomechanics and Modeling in Mechanobiology, 2011. 10(3): p. 371–382. [PubMed: 20628781]

17. Roberts MD, Sigal IA, Liang Y, Burgoyne CF, and Downs JC, Changes in the biomechanical response of the optic nerve head in early experimental glaucoma. Investigative Ophthalmology & Visual Science, 2010. 51(11): p. 5675–5684. [PubMed: 20538991]

18. Roberts MD, Grau V, Grimm J, Reynaud J, Bellezza AJ, Burgoyne CF, and Downs JC, Remodeling of the connective tissue microarchitecture of the lamina cribrosa in early experimental glaucoma. Investigative Ophthalmology & Visual Science, 2009. 50(2): p. 681–690. [PubMed: 18806292]

19. Voorhees AP, Jan N-J, and Sigal IA, Effects of collagen microstructure and material properties on the deformation of the neural tissues of the lamina cribrosa. Acta Biomaterialia, 2017. 58: p. 278–290. [PubMed: 28528864]

20. Sigal IA, Flanagan JG, Tertinegg I, and Ethier CR, Finite element modeling of optic nerve head biomechanics. Investigative Ophthalmology & Visual Science, 2004. 45(12): p. 4378–4387. [PubMed: 15557446]

21. Braunsmann C, Hammer CM, Rheinlaender J, Kruse FE, Schäffer TE, and Schlötzer-Schrehardt U, Evaluation of lamina cribrosa and peripapillary sclera stiffness in pseudoexfoliation and normal eyes by atomic force microscopy. Investigative Ophthalmology & Visual Science, 2012. 53(6): p. 2960–2967. [PubMed: 22491409]

22. Fazio MA, Grytz R, Bruno L, Girard MJ, Gardiner S, Girkin CA, and Downs JC, Regional variations in mechanical strain in the posterior human sclera. Investigative Ophthalmology & Visual Science, 2012. 53(9): p. 5326–5333. [PubMed: 22700704]

23. Quigley HA, Glaucoma: macrocosm to microcosm the Friedenwald lecture. Investigative Ophthalmology & Visual Science, 2005. 46(8): p. 2663–2670.

24. Sigal IA, Interactions between geometry and mechanical properties on the optic nerve head. Investigative Ophthalmology & Visual Science, 2009. 50(6): p. 2785–2795. [PubMed: 19168906]

25. Sigal IA, Yang H, Roberts MD, Burgoyne CF, and Downs JC, IOP-induced lamina cribrosa displacement and scleral canal expansion: an analysis of factor interactions using parameterized eye-specific models. Investigative Ophthalmology & Visual Science, 2011. 52(3): p. 1896–1907. [PubMed: 20881292]

26. Sigal IA, Flanagan JG, Tertinegg I, and Ethier CR, 3D morphometry of the human optic nerve head. Experimental Eye Research, 2010. 90(1): p. 70–80. [PubMed: 19772858]
27. Sigal IA, Grimm J, Schuman JS, Kagemann L, Ishikawa H, and Wollstein G, A method to estimate biomechanics and mechanical properties of optic nerve head tissues from parameters measurable using optical coherence tomography. IEEE Transactions on Medical Imaging, 2014. 33(6): p. 1381–1389. [PubMed: 24691117]
28. Hua Y, Voorhees AP, and Sigal IA, Cerebrospinal fluid pressure: revisiting factors influencing optic nerve head biomechanics. Investigative Ophthalmology & Visual Science, 2018. 59(1): p. 154–165. [PubMed: 29332130]
29. Jan N-J, Lathrop K, and Sigal IA, Collagen architecture of the posterior pole: high-resolution wide field of view visualization and analysis using polarized light microscopy. Investigative Ophthalmology & Visual Science, 2017. 58(2): p. 735–744. [PubMed: 28146238]
30. Lee P-Y, Yang B, and Sigal IA. Real-time measurement of collagen architecture and deformations at sub-micron resolution. in Summer Biomechanics, Bioengineering, and Biotransport Conference. 2019. Seven Springs, PA, USA.
31. Jan N-J, Brazile BL, Hu D, Grube G, Wallace J, Gogola A, and Sigal IA, Crimp around the globe; patterns of collagen crimp across the corneoscleral shell. Experimental Eye Research, 2018. 172: p. 159–170. [PubMed: 29660327]
32. Boote C, Sigal IA, Grytz R, Hua Y, Nguyen TD, and Girard MJ, Scleral structure and biomechanics. Progress in Retinal and Eye Research, 2020. 74: p. 100773. [PubMed: 31412277]
33. Bell J, Hayes S, Whitford C, Sanchez-Weatherby J, Shebanova O, Vergari C, Winlove C, Terrill N, Sorensen T, and Elsheikh A, The hierarchical response of human corneal collagen to load. Acta Biomaterialia, 2018. 65: p. 216–225. [PubMed: 29128531]
34. Bell JS, Hayes S, Whitford C, Sanchez-Weatherby J, Shebanova O, Terrill NJ, Sørensen TL, Elsheikh A, and Meek KM, Tropocollagen springs allow collagen fibrils to stretch elastically. Acta Biomaterialia, 2022. 142: p. 185–193. [PubMed: 35081430]
35. Komai Y and Ushiki T, The three-dimensional organization of collagen fibrils in the human cornea and sclera. Investigative Ophthalmology & Visual Science, 1991. 32(8): p. 2244–2258. [PubMed: 2071337]
36. Meek KM and Knupp C, Corneal structure and transparency. Progress in Retinal and Eye Research, 2015. 49: p. 1–16. [PubMed: 26145225]
37. Quantock AJ, Winkler M, Parfitt GJ, Young RD, Brown DJ, Boote C, and Jester JV, From nano to macro: studying the hierarchical structure of the corneal extracellular matrix. Experimental Eye Research, 2015. 133: p. 81–99. [PubMed: 25819457]
38. Lee P-Y, Yang B, Hua Y, Waxman S, Zhu Z, Ji F, and Sigal IA, Real-time imaging of optic nerve head collagen microstructure and biomechanics using instant polarized light microscopy. Experimental Eye Research, 2022. 217: p. 108967. [PubMed: 35114213]
39. Yang B, Lee PY, Hua Y, Brazile B, Waxman S, Ji F, Zhu Z, and Sigal IA, Instant polarized light microscopy for imaging collagen microarchitecture and dynamics. Journal of Biophotonics, 2021. 14(2): p. e202000326. [PubMed: 33103363]
40. Lee P-Y, Yang B, and Sigal IA, Polarization microscopy, in Optical Elastography: Optical Techniques for Assessing Cell and Tissue Biomechanics. 2023, SPIE Press.
41. Schindelin J, Arganda-Carreras I, Frise E, Kaynig V, Longair M, Pietzsch T, Preibisch S, Rueden C, Saalfeld S, and Schmid B, Fiji: an open-source platform for biological-image analysis. Nature Methods, 2012. 9(7): p. 676–682. [PubMed: 22743772]
42. Jan N-J, Grimm JL, Tran H, Lathrop KL, Wollstein G, Bilonick RA, Ishikawa H, Kagemann L, Schuman JS, and Sigal IA, Polarization microscopy for characterizing fiber orientation of ocular tissues. Biomedical Optics Express, 2015. 6(12): p. 4705–4718. [PubMed: 26713188]
43. Zhong F and Quan C, Efficient digital image correlation using gradient orientation. Optics & Laser Technology, 2018. 106: p. 417–426.
44. Jammalamadaka SR and Sengupta A, Topics in circular statistics. Vol. 5. 2001: world scientific.
45. Team RC, R: A language and environment for statistical computing. 2022, R Foundation for Statistical Computing.

46. Hill MR, Duan X, Gibson GA, Watkins S, and Robertson AM, A theoretical and non-destructive experimental approach for direct inclusion of measured collagen orientation and recruitment into mechanical models of the artery wall. Journal of Biomechanics, 2012. 45(5): p. 762–771. [PubMed: 22305290]
47. Holzapfel GA, Biomechanics of soft tissue. The handbook of materials behavior models, 2001. 3: p. 1049–1063.
48. Grytz R and Meschke G, Constitutive modeling of crimped collagen fibrils in soft tissues. Journal of the Mechanical Behavior of Biomedical Materials, 2009. 2(5): p. 522–533. [PubMed: 19627859]
49. Hansen KA, Weiss JA, and Barton JK, Recruitment of tendon crimp with applied tensile strain. Journal of Biomechanical Engineering, 2002. 124(1): p. 72–77. [PubMed: 11871607]
50. Thornton G, Shrive N, and Frank C, Ligament creep recruits fibres at low stresses and can lead to modulus-reducing fibre damage at higher creep stresses: a study in rabbit medial collateral ligament model. Journal of Orthopaedic Research, 2002. 20(5): p. 967–974. [PubMed: 12382961]
51. Foong TY, Hua Y, Amini R, and Sigal IA, Who bears the load? IOP-induced collagen fiber recruitment over the corneoscleral shell. Experimental Eye Research, 2023: p. 109446. [PubMed: 36935071]
52. Pavlatos E, Perez BC, Morris HJ, Chen H, Palko JR, Pan X, Weber PA, Hart RT, and Liu J, Three-dimensional strains in human posterior sclera using ultrasound speckle tracking. Journal of Biomechanical Engineering, 2016. 138(2): p. 021015. [PubMed: 26632258]
53. Ma Y, Pavlatos E, Clayson K, Kwok S, Pan X, and Liu J, Three-dimensional inflation response of porcine optic nerve head using high-frequency ultrasound elastography. Journal of Biomechanical Engineering, 2020. 142(5): p. 051013. [PubMed: 31750882]
54. Dale W, Baer E, Keller A, and Kohn R, On the ultrastructure of mammalian tendon. Experientia, 1972. 28: p. 1293–1295. [PubMed: 4638892]
55. Diamant J, Keller A, Baer E, Litt M, and Arridge R, Collagen; ultrastructure and its relation to mechanical properties as a function of ageing. Proceedings of the Royal Society of London. Series B. Biological Sciences, 1972. 180(1060): p. 293–315. [PubMed: 4402469]
56. Yang W, Sherman VR, Gludovatz B, Schaible E, Stewart P, Ritchie RO, and Meyers MA, On the tear resistance of skin. Nature Communications, 2015. 6(1): p. 6649.
57. Gregory J, Hazel AL, and Shearer T, A microstructural model of tendon failure. Journal of the mechanical behavior of biomedical materials, 2021. 122: p. 104665. [PubMed: 34311323]
58. Bevan T, Merabet N, Hornsby J, Watton PN, and Thompson MS, A biomechanical model for fibril recruitment: evaluation in tendons and arteries. Journal of Biomechanics, 2018. 74: p. 192–196. [PubMed: 29636179]
59. Grytz R and Meschke G, A computational remodeling approach to predict the physiological architecture of the collagen fibril network in corneo-scleral shells. Biomechanics and Modeling in Mechanobiology, 2010. 9(2): p. 225–235. [PubMed: 19802726]
60. Coudrillier B, Boote C, Quigley HA, and Nguyen TD, Scleral anisotropy and its effects on the mechanical response of the optic nerve head. Biomechanics and Modeling in Mechanobiology, 2013. 12(5): p. 941–963. [PubMed: 23188256]
61. Franchi M, Ottani V, Stagni R, and Ruggeri A, Tendon and ligament fibrillar crimps give rise to left-handed helices of collagen fibrils in both planar and helical crimps. Journal of Anatomy, 2010. 216(3): p. 301–309. [PubMed: 20070421]
62. Franchi M, Fini M, Quaranta M, De Pasquale V, Raspanti M, Giavaresi G, Ottani V, and Ruggeri A, Crimp morphology in relaxed and stretched rat Achilles tendon. Journal of Anatomy, 2007. 210(1): p. 1–7. [PubMed: 17229278]
63. Fratzl P, Collagen: structure and mechanics, an introduction, in Collagen. 2008, Springer. p. 1–13.
64. Brazile BL, Hua Y, Jan N-J, Wallace J, Gogola A, and Sigal IA, Thin lamina cribrosa beams have different collagen microstructure than thick beams. Investigative Ophthalmology & Visual Science, 2018. 59(11): p. 4653–4661. [PubMed: 30372734]
65. Grytz R, Krishnan K, Whitley R, Libertiaux V, Sigal IA, Girkin CA, and Downs JC, A mesh-free approach to incorporate complex anisotropic and heterogeneous material properties into

eye-specific finite element models. Computer Methods in Applied Mechanics and Engineering, 2020. 358: p. 112654.

66. Grytz R, Girkin CA, Libertiaux V, and Downs JC, Perspectives on biomechanical growth and remodeling mechanisms in glaucoma. Mechanics Research Communications, 2012. 42: p. 92–106. [PubMed: 23109748]
67. Girard MJ, Suh J-KF, Bottlang M, Burgoyne CF, and Downs JC, Biomechanical changes in the sclera of monkey eyes exposed to chronic IOP elevations. Investigative Ophthalmology & Visual Science, 2011. 52(8): p. 5656–5669. [PubMed: 21519033]
68. Grytz R, Yang H, Hua Y, Samuels BC, and Sigal IA, Connective tissue remodeling in myopia and its potential role in increasing risk of glaucoma. Current Opinion in Biomedical Engineering, 2020. 15: p. 40–50. [PubMed: 32211567]
69. Girard MJ, Downs JC, Bottlang M, Burgoyne CF, and Suh J-KF, Peripapillary and posterior scleral mechanics—part II: experimental and inverse finite element characterization. Journal of Biomechanical Engineering, 2009. 131(5): p. 051012. [PubMed: 19388782]
70. Perez BC, Tang J, Morris HJ, Palko JR, Pan X, Hart RT, and Liu J, Biaxial mechanical testing of posterior sclera using high-resolution ultrasound speckle tracking for strain measurements. Journal of Biomechanics, 2014. 47(5): p. 1151–1156. [PubMed: 24438767]
71. Wang S and Hatami-Marbini H, Constitutive modeling of corneal tissue: influence of three-dimensional collagen fiber microstructure. Journal of Biomechanical Engineering, 2021. 143(3).
72. Miller KM and Quigley HA, The clinical appearance of the lamina cribrosa as a function of the extent of glaucomatous optic nerve damage. Ophthalmology, 1988. 95(1): p. 135–138. [PubMed: 3344121]
73. Schuman JS, Kostanyan T, and Bussel I, Review of longitudinal glaucoma progression: 5 years after the shaffer lecture. Ophthalmology Glaucoma, 2020. 3(2): p. 158–166. [PubMed: 32373782]
74. Jones H, Girard M, White N, Fautsch M, Morgan J, Ethier C, and Albon J, Quantitative analysis of three-dimensional fibrillar collagen microstructure within the normal, aged and glaucomatous human optic nerve head. Journal of the Royal Society Interface, 2015. 12(106): p. 20150066. [PubMed: 25808336]
75. Sugita M, Pircher M, Zotter S, Baumann B, Roberts P, Makihira T, Tomatsu N, Sato M, Vass C, and Hitzenberger CK, Retinal nerve fiber bundle tracing and analysis in human eye by polarization sensitive OCT. Biomedical Optics Express, 2015. 6(3): p. 1030–1054. [PubMed: 25798324]
76. Kamma-Lorger CS, Boote C, Hayes S, Moger J, Burghammer M, Knupp C, Quantock AJ, Sorensen T, Di Cola E, and White N, Collagen and mature elastic fibre organisation as a function of depth in the human cornea and limbus. Journal of Structural Biology, 2010. 169(3): p. 424–430. [PubMed: 19914381]
77. Ho LC, Sigal IA, Jan N-J, Squires A, Tse Z, Wu EX, Kim S-G, Schuman JS, and Chan KC, Magic angle–enhanced MRI of fibrous microstructures in sclera and cornea with and without intraocular pressure loading. Investigative Ophthalmology & Visual Science, 2014. 55(9): p. 5662–5672. [PubMed: 25103267]
78. Wu J, Rajwa B, Filmer DL, Hoffmann CM, Yuan B, Chiang C-S, Sturgis J, and Robinson JP, Analysis of orientations of collagen fibers by novel fiber-tracking software. Microscopy and Microanalysis, 2003. 9(6): p. 574–580. [PubMed: 14750992]
79. Cheng F, Birder LA, Kullmann FA, Hornsby J, Watton PN, Watkins S, Thompson M, and Robertson AM, Layer-dependent role of collagen recruitment during loading of the rat bladder wall. Biomechanics and Modeling in Mechanobiology, 2018. 17(2): p. 403–417. [PubMed: 29039043]
80. McQuaid R, Li J, Cummings A, Mrochen M, and Vohnsen B, Second-harmonic reflection imaging of normal and accelerated corneal crosslinking using porcine corneas and the role of intraocular pressure. Cornea, 2014. 33(2): p. 125–130. [PubMed: 24322797]
81. Spiesz EM, Thorpe CT, Thurner PJ, and Screen HR, Structure and collagen crimp patterns of functionally distinct equine tendons, revealed by quantitative polarised light microscopy (qPLM). Acta Biomaterialia, 2018. 70: p. 281–292. [PubMed: 29409868]
82. Sharabi M, Structural mechanisms in soft fibrous tissues: A review. Frontiers in Materials, 2022. 8: p. 793647.

83. Pissarenko A, Ruestes CJ, and Meyers MA, Constitutive description of skin dermis: Through analytical continuum and coarse-grained approaches for multi-scale understanding. Acta biomaterialia, 2020. 106: p. 208–224. [PubMed: 32014584]
84. Shearer T, Parnell WJ, Lynch B, Screen HR, and David Abrahams I, A recruitment model of tendon viscoelasticity that incorporates fibril creep and explains strain-dependent relaxation. Journal of biomechanical engineering, 2020. 142(7): p. 071003. [PubMed: 34043761]
85. Khoffi F and Heim F, Mechanical degradation of biological heart valve tissue induced by low diameter crimping: an early assessment. Journal of The Mechanical Behavior of Biomedical Materials, 2015. 44: p. 71–75. [PubMed: 25621851]
86. Davidson CD, Jayco DKP, Wang WY, Shikanov A, and Baker BM, Fiber crimp confers matrix mechanical nonlinearity, regulates endothelial cell mechanosensing, and promotes microvascular network formation. Journal of Biomechanical Engineering, 2020. 142(11): p. 111009. [PubMed: 32839824]
87. Legerlotz K, Dorn J, Richter J, Rausch M, and Leupin O, Age-dependent regulation of tendon crimp structure, cell length and gap width with strain. Acta Biomaterialia, 2014. 10(10): p. 4447–4455. [PubMed: 24907659]
88. Freedman BR, Zuskov A, Sarver JJ, Buckley MR, and Soslowsky LJ, Evaluating changes in tendon crimp with fatigue loading as an ex vivo structural assessment of tendon damage. Journal of Orthopaedic Research, 2015. 33(6): p. 904–910. [PubMed: 25773654]
89. Niestrawska JA, Pukaluk A, Babu AR, and Holzapfel GA, Differences in collagen fiber diameter and waviness between healthy and aneurysmal abdominal aortas. Microscopy and Microanalysis, 2022. 28(5): p. 1649–1663.
90. Siadat SM and Ruberti JW, Mechanochemistry of collagen. Acta Biomaterialia, 2023.
91. Gogola A, Jan N-J, Lathrop KL, and Sigal IA, Radial and circumferential collagen fibers are a feature of the peripapillary sclera of human, monkey, pig, cow, goat, and sheep. Investigative Ophthalmology & Visual Science, 2018. 59(12): p. 4763–4774. [PubMed: 30304458]
92. Candia OA, Gerometta RM, and Danias J, Tissue plasminogen activator reduces the elevated intraocular pressure induced by prednisolone in sheep. Experimental Eye Research, 2014. 128: p. 114–116. [PubMed: 25304217]
93. Gerometta R, Spiga M-G, Borrás T, and Candia OA, Treatment of sheep steroid–induced ocular hypertension with a glucocorticoid-inducible MMP1 gene therapy virus. Investigative Ophthalmology & Visual Science, 2010. 51(6): p. 3042–3048. [PubMed: 20089869]
94. Brooks DE, Arellano E, Kubilis PS, and Komaromy AM, Histomorphometry of the porcine scleral lamina cribrosa surface. Veterinary Ophthalmology, 1998. 1(2–3): p. 129–135. [PubMed: 11397222]
95. A Bouhenni R, Dunmire J, Sewell A, and Edward DP, Animal models of glaucoma. BioMed Research International, 2012. 2012.
96. Yang B, Jan NJ, Brazile B, Voorhees A, Lathrop KL, and Sigal IA, Polarized light microscopy for 3-dimensional mapping of collagen fiber architecture in ocular tissues. Journal of Biophotonics, 2018. 11(8): p. e201700356. [PubMed: 29633576]
97. Yang B, Brazile B, Jan N-J, Hua Y, Wei J, and Sigal IA, Structured polarized light microscopy for collagen fiber structure and orientation quantification in thick ocular tissues. Journal of Biomedical Optics, 2018. 23(10): p. 106001. [PubMed: 30277032]
98. Gusachenko I, Latour G, and Schanne-Klein M-C, Polarization-resolved Second Harmonic microscopy in anisotropic thick tissues. Optics Express, 2010. 18(18): p. 19339–19352. [PubMed: 20940829]
99. Voorhees AP, Jan NJ, and Sigal IA, Effects of collagen microstructure and material properties on the deformation of the neural tissues of the lamina cribrosa. Acta Biomater, 2017. 58: p. 278–290. [PubMed: 28528864]
100. Zhang L, Albon J, Jones H, Gouget CL, Ethier CR, Goh JC, and Girard MJ, Collagen microstructural factors influencing optic nerve head biomechanics. Investigative Ophthalmology & Visual Science, 2015. 56(3): p. 2031–2042. [PubMed: 25736791]

101. Pinsky PM, Van Der Heide D, and Chernyak D, Computational modeling of mechanical anisotropy in the cornea and sclera. Journal of Cataract & Refractive Surgery, 2005. 31(1): p. 136–145. [PubMed: 15721706]
102. Vasta M, Gizzi A, and Pandolfi A, On three-and two-dimensional fiber distributed models of biological tissues. Probabilistic Engineering Mechanics, 2014. 37: p. 170–179.
103. Gizzi A, Vasta M, and Pandolfi A, Modeling collagen recruitment in hyperelastic bio-material models with statistical distribution of the fiber orientation. International Journal of Engineering Science, 2014. 78: p. 48–60.
104. Cheng X, Petsche SJ, and Pinsky PM, A structural model for the in vivo human cornea including collagen-swelling interaction. Journal of The Royal Society Interface, 2015. 12(109): p. 20150241. [PubMed: 26156299]
105. Gizzi A, Pandolfi A, and Vasta M, Statistical characterization of the anisotropic strain energy in soft materials with distributed fibers. Mechanics of Materials, 2016. 92: p. 119–138.
106. Voorhees AP, Jan N-J, Hua Y, Yang B, and Sigal IA, Peripapillary sclera architecture revisited: a tangential fiber model and its biomechanical implications. Acta Biomaterialia, 2018. 79: p. 113–122. [PubMed: 30142444]
107. Wang R, Mattson JM, and Zhang Y, Effect of aging on the biaxial mechanical behavior of human descending thoracic aorta: Experiments and constitutive modeling considering collagen crosslinking. Journal of the Mechanical Behavior of Biomedical Materials, 2023. 140: p. 105705. [PubMed: 36758423]
108. Wagner DR and Lotz JC, Theoretical model and experimental results for the nonlinear elastic behavior of human annulus fibrosus. Journal of Orthopaedic Research, 2004. 22(4): p. 901–909. [PubMed: 15183453]
109. Hatami-Marbini H and Pachenari M, Hydration related changes in tensile response of posterior porcine sclera. Journal of the Mechanical Behavior of Biomedical Materials, 2020. 104: p. 103562. [PubMed: 32174383]
110. Pachenari M and Hatami-Marbini H, Regional differences in the glycosaminoglycan role in porcine scleral hydration and mechanical behavior. Investigative Ophthalmology & Visual Science, 2021. 62(3): p. 28–28.
111. El Hamdaoui M, Levy AM, Stuber AB, Girkin CA, Kraft TW, Samuels BC, and Grytz R, Scleral crosslinking using genipin can compromise retinal structure and function in tree shrews. Experimental Eye Research, 2022. 219: p. 109039. [PubMed: 35339475]
112. Chang S-H, Zhou D, Eliasy A, Li Y-C, and Elsheikh A, Experimental evaluation of stiffening effect induced by UVA/Riboflavin corneal cross-linking using intact porcine eye globes. Plos One, 2020. 15(11): p. e0240724. [PubMed: 33147249]
113. Luo Y, Duprey A, Avril S, and Lu J, Characteristics of thoracic aortic aneurysm rupture in vitro. Acta Biomaterialia, 2016. 42: p. 286–295. [PubMed: 27395826]
114. Mattson JM, Wang Y, and Zhang Y, Contributions of glycosaminoglycans to collagen fiber recruitment in constitutive modeling of arterial mechanics. Journal of Biomechanics, 2019. 82: p. 211–219. [PubMed: 30415914]
115. Cheng F, Watton PN, Pederzani G, Kurobe M, Takaoka E.-i., Chapple C, Birder L, Yoshimura N, and Robertson AM, A constrained mixture-micturition-growth (CMMG) model of the urinary bladder: Application to partial bladder outlet obstruction (BOO). Journal of The Mechanical Behavior of Biomedical Materials, 2022. 134: p. 105337. [PubMed: 35863296]
116. Sigal IA and Grimm JL, A few good responses: which mechanical effects of IOP on the ONH to study? Investigative Ophthalmology & Visual Science, 2012. 53(7): p. 4270–4278. [PubMed: 22570343]
117. Sigal IA, Grimm JL, Jan N-J, Reid K, Minckler DS, and Brown DJ, Eye-specific IOP-induced displacements and deformations of human lamina cribrosa. Investigative Ophthalmology & Visual Science, 2014. 55(1): p. 1–15. [PubMed: 24334450]
118. Girard MJ, Beotra MR, Chin KS, Sandhu A, Clemo M, Nikita E, Kamal DS, Papadopoulos M, Mari JM, and Aung T, In vivo 3-dimensional strain mapping of the optic nerve head following intraocular pressure lowering by trabeculectomy. Ophthalmology, 2016. 123(6): p. 1190–1200. [PubMed: 26992836]

119. Wang R, Raykin J, Gleason RL Jr, and Ethier CR, Residual deformations in ocular tissues. Journal of The Royal Society Interface, 2015. 12(105): p. 20141101. [PubMed: 25740853]

120. Grytz R and Downs JC, A forward incremental prestressing method with application to inverse parameter estimations and eye-specific simulations of posterior scleral shells. Computer Methods in Biomechanics and Biomedical Engineering, 2013. 16(7): p. 768–780. [PubMed: 22224843]

Statement of Significance:

Peripapillary sclera (PPS) and lamina cribrosa (LC) collagen recruitment behaviors are central to the nonlinear mechanical behavior of the posterior pole of the eye. How PPS and LC collagen fibers recruit under stretch is crucial to develop constitutive models of the tissues but remains unclear. We used image-based stretch testing to characterize PPS and LC collagen fiber bundle recruitment under local stretch. We found that fiber-level stretch-recruitment curves of PPS and LC approximated sigmoid functions. PPS recruited more fibers at a low stretch, but at 10% bundle stretch the two curves crossed with 75% bundles recruited. We also found that PPS and LC fibers had different uncrimping rates and non-zero waviness's when recruited.

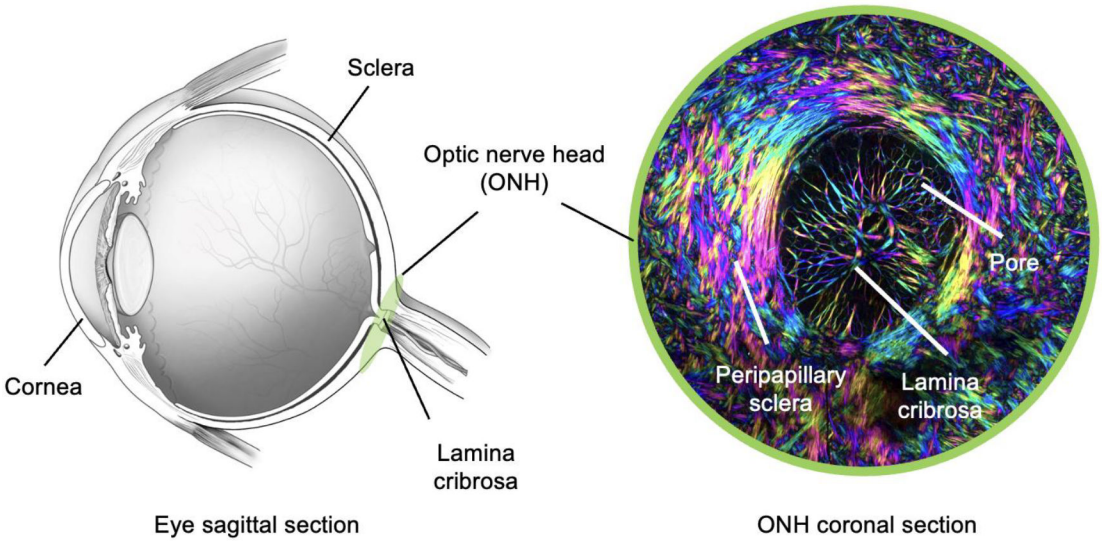

Figure 1.

The anatomy of the eye and optic nerve head (ONH). (Left) A sagittal view of an eye is shown. Adapted from a diagram by the National Eye Institute. (Right) A coronal view of ONH acquired by instant polarized light microscopy. The image encodes pixel-level collagen fiber orientation and density as hue and brightness, respectively. The lamina cribrosa (LC) is a mesh-like connective tissue spanning the scleral canal. Through the pores of the LC pass the retinal ganglion cell axons that carry visual information from the eye to the brain and blood vessels that perfuse the posterior pole.

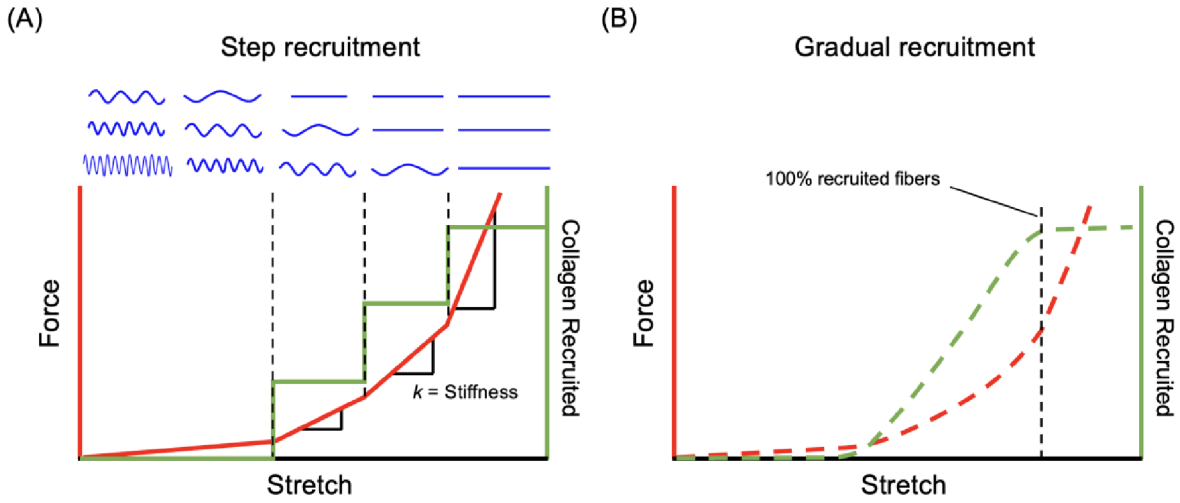

Figure 2.

Schematic illustration of how the collagen crimp determines the nonlinear mechanical behavior of a fiber bundle. A wavy fiber is not recruited. Conversely, a fiber that is straightened is recruited. (A) In a simple recruitment model, a collagen fiber bundle consists of several fibers with variable crimp (blue curves). When no fiber is recruited, the fiber bundle has a low stretch-force slope, i.e., low stiffness. Fibers become recruited one by one as stretch increases (green curve). Step recruitment results in an abrupt, step, increase in stiffness (red curve). (B) When a fiber bundle consists of many fibers with variable crimp. A progressively increasing fraction of fibers becomes recruited as stretch increases (green curve). Gradual recruitment leads to a nonlinear increase in stiffness (red curve). When all fibers are recruited (black dash), the stiffness, i.e., stretch-force slope, becomes a constant. Actual tissues exhibit an even more complex process, with fibers rotating, interacting with one another, for instance through crosslinks, are interlocked and can slide. Nevertheless, several tissues have been shown to follow closely the recruitment process described here. [46, 113]

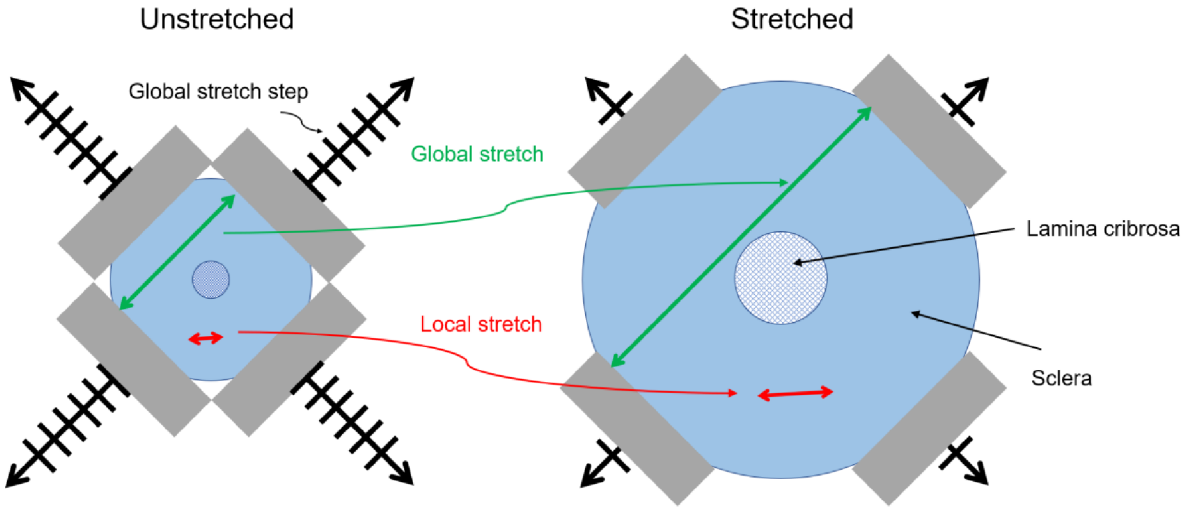

Figure 3.

Schematic of biaxial stretch testing. Clamps (grey rectangles) mounted and stretched an ONH section (blue donut) equally along two orthogonal axes. Global stretch was defined as the change in clamp-to-clamp distance (green arrow) as the sample was stretched. Each global stretch step was 0.5 mm. Local stretch was calculated by the percent length change in the region of interest (red arrow) on the PPS or LC fiber bundles tracking by digital image correlation. Note that the amount of stretch is exaggerated for clarity.

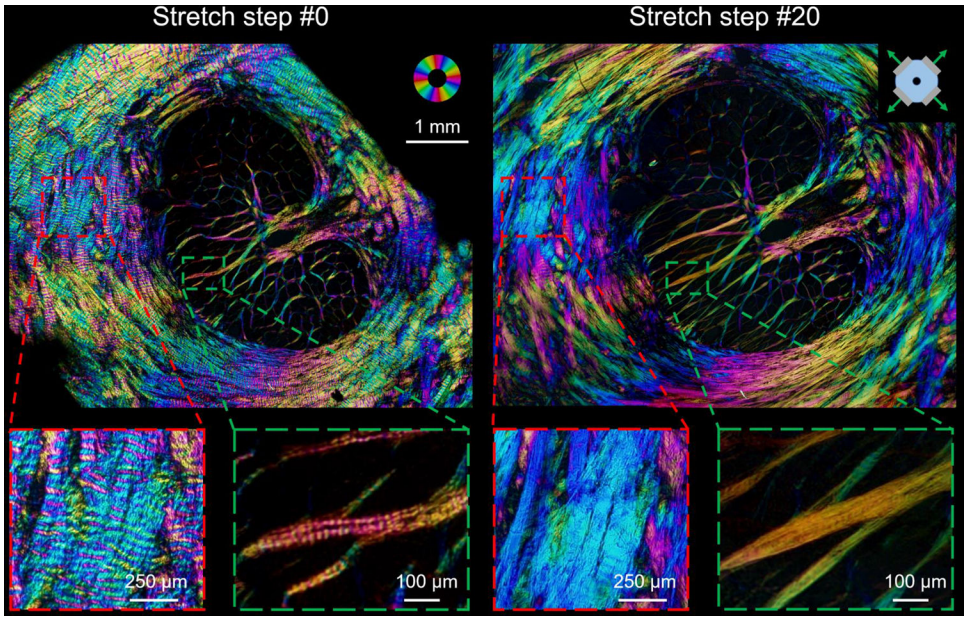

Figure 4.

Collagen crimp visualization in the ONH. IPOL image mosaics of a coronal section from the ONH of an unfixed sheep eye under a quasi-static biaxial stretch. On the left hand as mounted before stretch (Stretch step 0). On the right hand after stretch (Stretch step #20). The color disc on the top right-hand side of the image represents local fiber orientation, and the brightness of each pixel in the images represents local fiber density. The bottom row shows close-ups of PPS (left) and LC (right) in each condition. The dark shadows on the corners of the top left panel indicate the locations of the clamps. Using the IPOL technique allowed identifying the difference in collagen microstructure such as crimp before and after stretch. At the initial state, PPS and LC collagen fibers had clear waviness, discernible by the color bands. In contrast, at the stretched state, there were far fewer undulations in color on the PPS and LC collagen fibers, indicative of straightened, recruited fibers. A perfectly straight fiber has a single orientation and therefore a single color. Note the large changes in the canal shape, starting as elliptical and finishing close to circular.

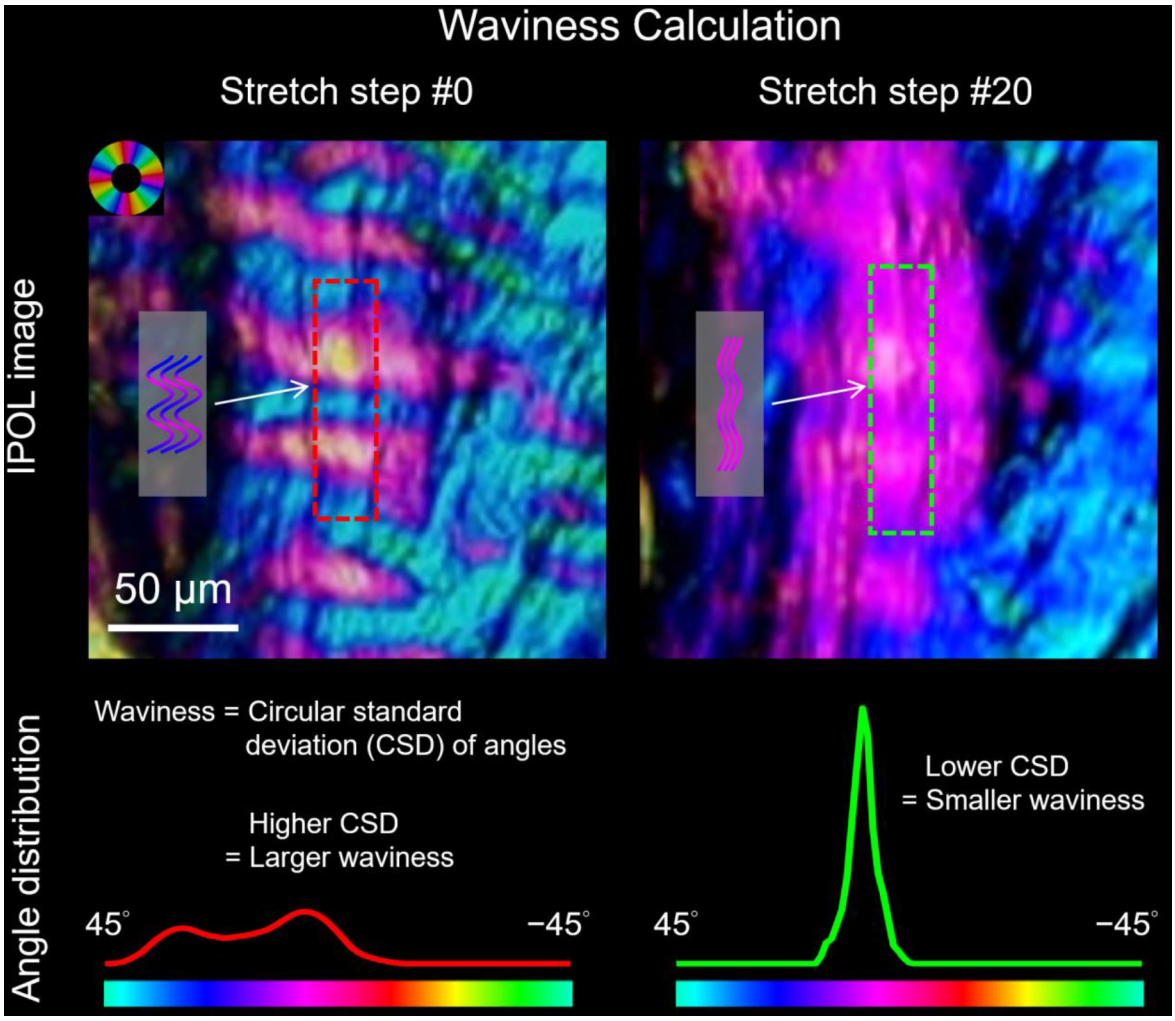

Figure 5.

IPOL images of PPS collagen and their corresponding orientation distributions within a region of interest (dashed rectangle) at different stretch states. Waviness was calculated using the circular standard deviation of the collagen fiber orientations. In wavy crimped fiber bundles, the orientation distribution is more variable, resulting in larger waviness values (left) whereas in recruited fibers, the distribution is less variable, resulting in smaller waviness values (right). Local stretch was the percent change in the long axis between two regions of interest (red dash rectangle to green dash rectangle) on the fiber bundles, where the displacements of the long axis were measured by digital image correlation. [43]

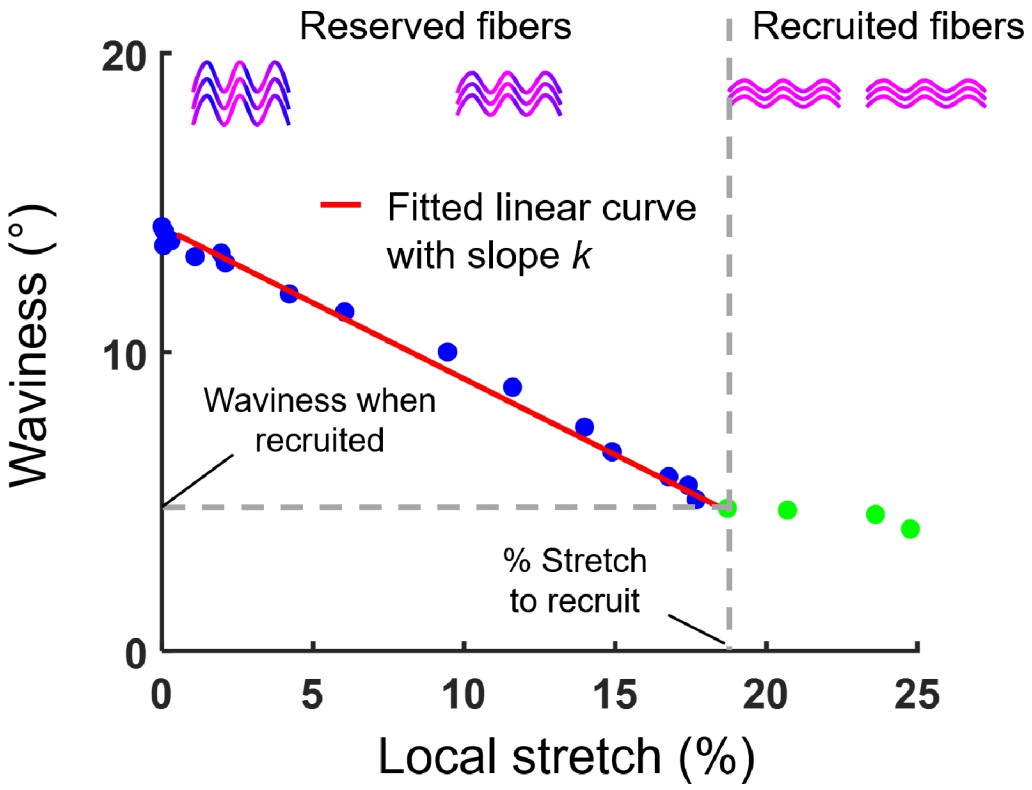

Figure 6.

Local waviness-stretch curve. Local stretch represents the elongation in the local region. This is different from the clamp-to-clamp biaxial stretch of the entire ONH. As the local stretch increased, the waviness of collagen fibers of the posterior pole decreased. Fiber recruitment was defined as when the waviness of collagen fibers remains constant despite further increases in local stretch. The values at that point are the “waviness when recruited” and “% stretch to recruit”. The waviness-stretch curve until recruited was fitted using linear regression. The absolute magnitude of the slope *k* of the fitted line was defined as the “uncrimping rate”.

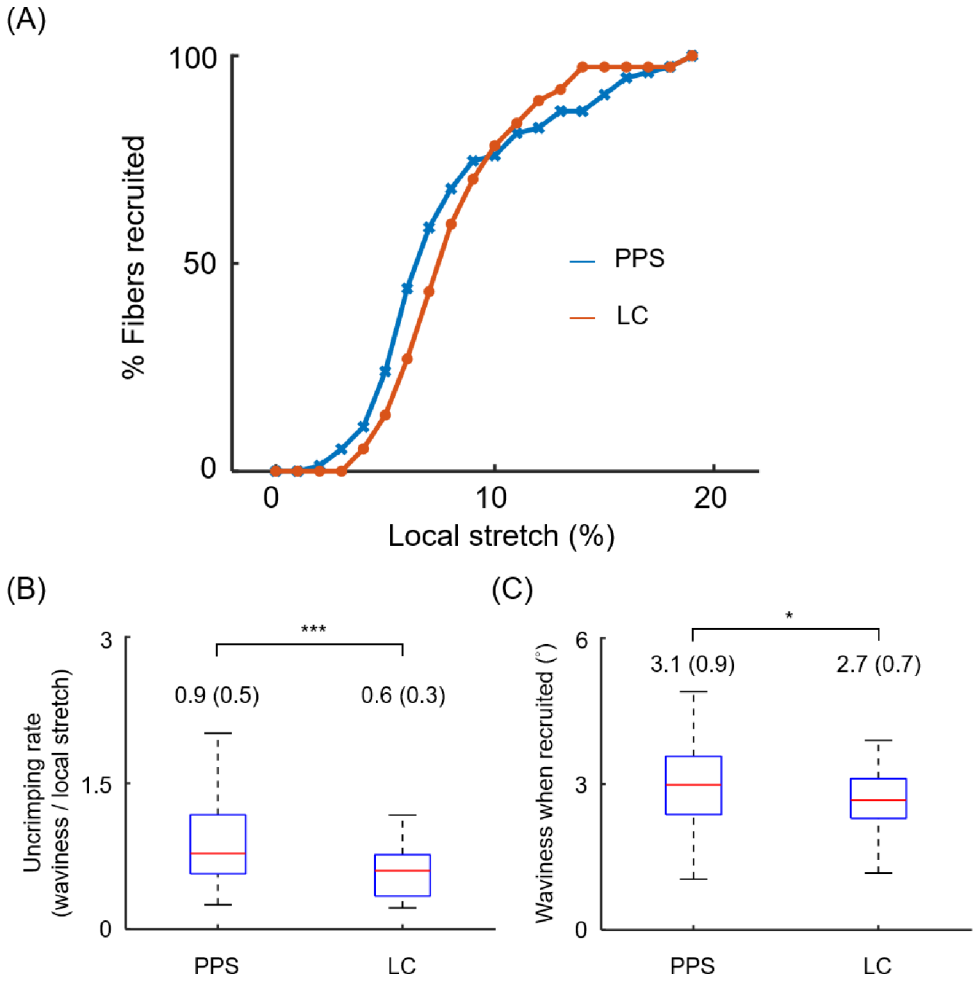

Figure 7.

Collagen fiber recruitment curves of PPS and LC under local stretch. (A) A total of 75 PPS collagen bundles and 37 LC beams were recruited under stretch testing. Local stretch-recruitment curves are plotted based on the measurements “% stretch to recruit” of PPS and LC. Both curves approximated a sigmoid function. About 75% of PPS and LC fibers were recruited at a 10% local stretch. The PPS recruited more fibers than the LC when the local stretch was less than 10%. (B) Boxplot of uncrimping rates in the PPS and LC beams. Average (standard deviation) uncrimping rates for PPS and LC beams are labeled above the whisker’s tip. PPS beams had a significantly higher uncrimping rate (P’s < 0.001). (C) Boxplot of waviness when recruited in the PPS and LC beams. Average (standard deviation) waviness when recruited for PPS and LC beams are labeled above the whisker’s tip. The waviness when recruited of the collagen fiber in the PPS was larger and more variable than that of the LC (P’s < 0.05).

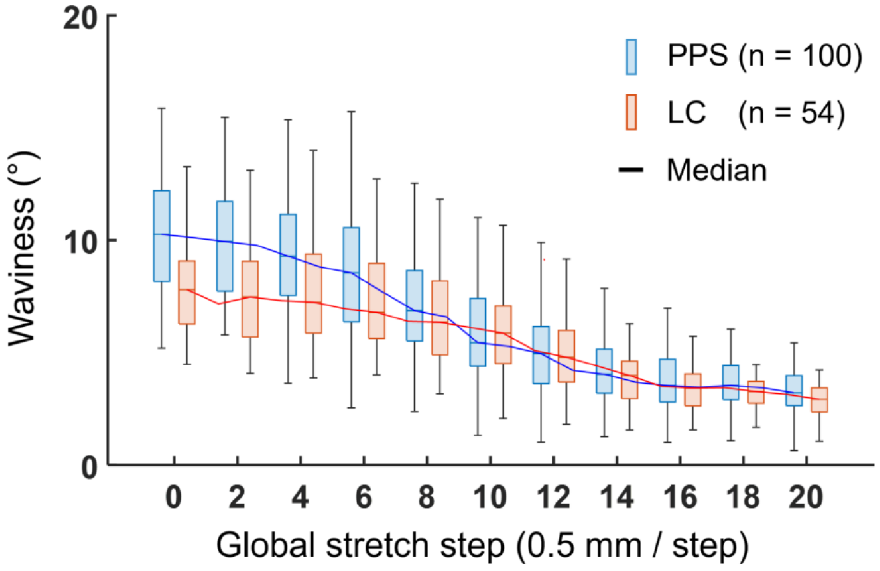

Figure 8.

Collagen waviness of the PPS and LC decreased with global stretch. Each stretch step was 0.5 mm for an ONH section isolated using an 11-mm-diameter trephine. At each stretch step, we measured the distributions of the collagen crimp waviness in the PPS (blue) and LC (orange), represented here as thin box plots. The median of the waviness at each stretch step was connected to highlight the differences between PPS and LC. A total of 154 measurements of waviness were collected, of which 100 were of PPS collagen bundles and 54 of LC beams across all sections. At the initial state, the average (SD) waviness measurements were 10.4° (2.7°) for PPS beams and 8.3° (2.6°) for LC beams, showing that the waviness in the PPS was significantly higher than the waviness in the LC (P's < 0.001). At the fully stretched state, the average (SD) waviness measurements were 3.5° (1.2°) for PPS beams and 3.3° (1.2°) for LC beams, showing that there was no significant difference between the waviness in the PPS and LC.

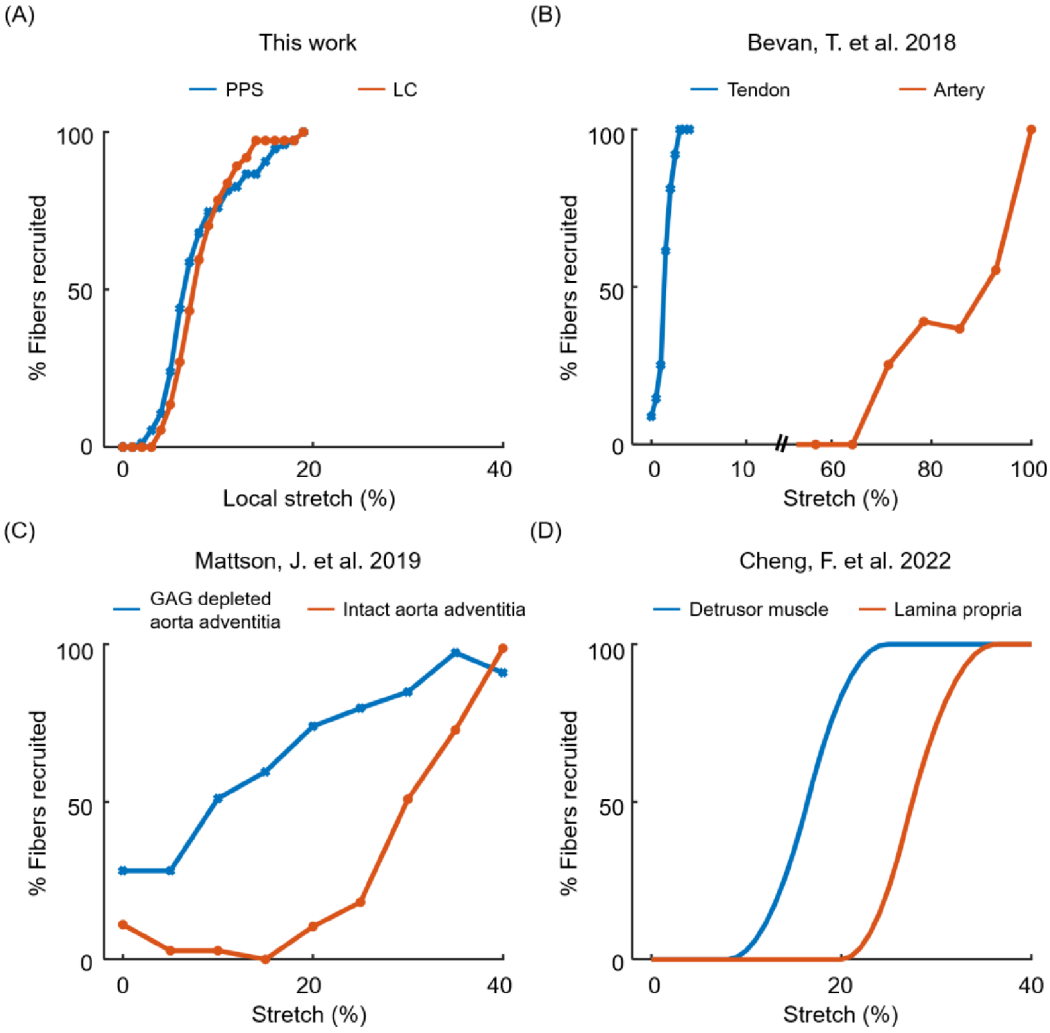

Figure 9.

Collagen fiber recruitment curves as a function of stretch for various collagenous soft tissues. Shown are (A) the PPS and LC in the sheep optic nerve head obtained in this work, (B) rat tail tendon and porcine aortic arteries [58], (C) porcine thoracic intact and glycosaminoglycan (GAG) depleted aorta [114], and (D) detrusor muscle and lamina propria in the rat bladder [115]. The curves in Panel D were estimated based on the parameters provided for a triangular probability density function.

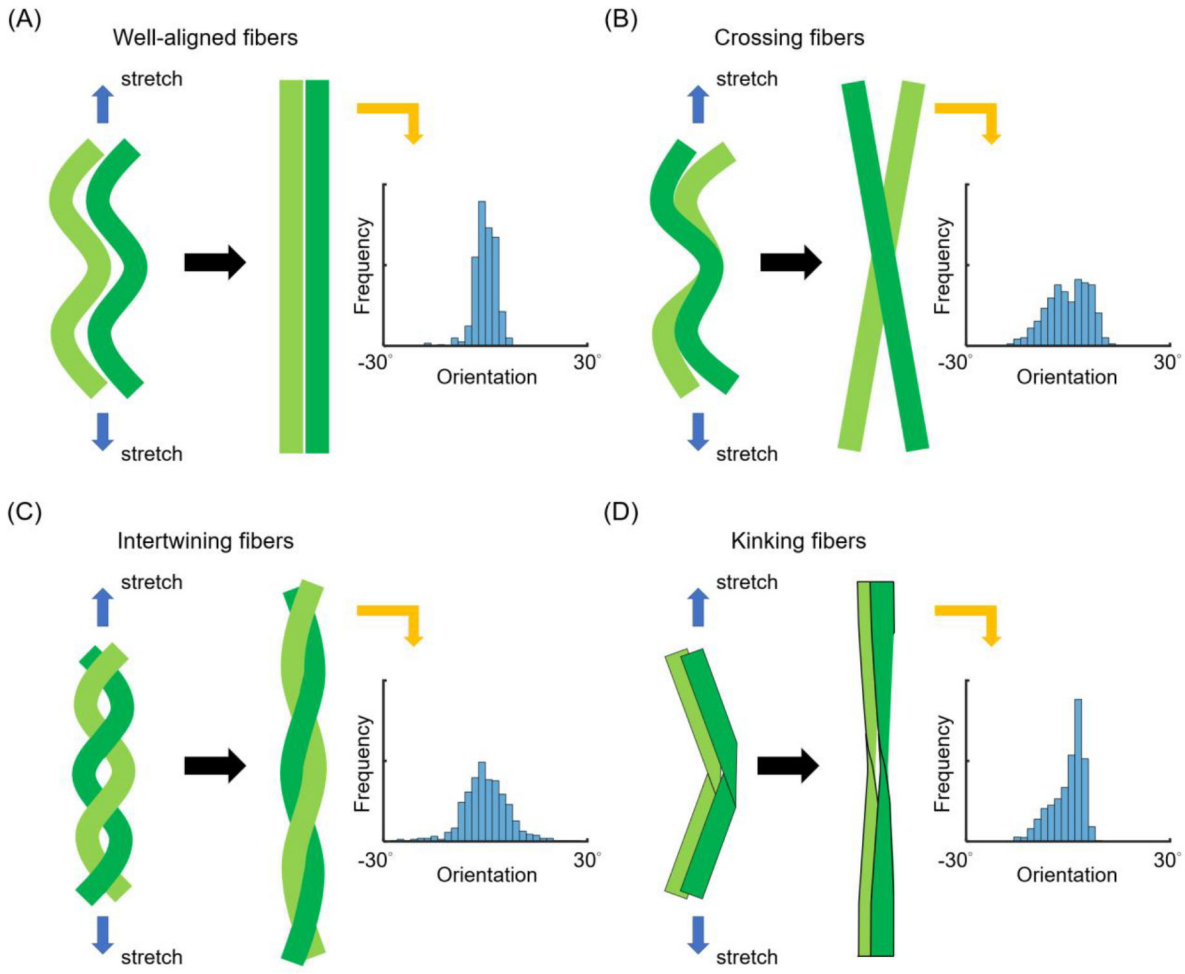

Figure 10.

Illustrative examples of how the microstructure at the fiber scale can result in non-zero waviness even under full recruitment. (A) Ideal fiber recruitment indicates that fibers are well-aligned, with a narrow distribution of orientations and a near-zero waviness. When fibers are (B) crossed (i.e., a distribution with two peaks), (C) intertwined (i.e., a wide distribution), or (D) kinked (i.e., a skewed distribution), fibers never lose their structural identity under stretching and thus still present residual waviness even when fully loaded and maximally recruited. In such cases, waviness when recruited is larger than zero. Therefore, waviness when recruited and its corresponding angle distribution may reflect how a fiber microstructure differs from a well-aligned one. Note that despite the excellent resolution of IPOL, it is still not sufficient to directly identify such sub-microstructures.

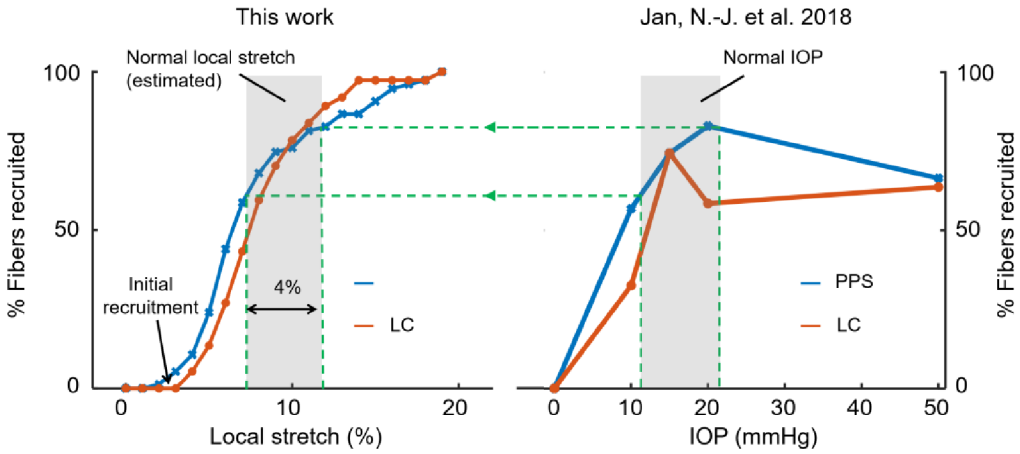

Figure 11.

Comparison of the collagen recruitment curves of the PPS (blue lines) and LC (red lines) as a function of stretch obtained in this work (Left) and as a function of IOP from a previous study (Right) [14]. Please see the main text for more details on the similarities and differences between the studies. Both studies found increased fractions of fibers recruited with increased IOP or stretch, as expected. In both cases, the tissues of the PPS recruited at slightly lower magnitudes of the input than the tissues of the LC. This direct side-by-side comparison allows an interesting observation: looking at the IOP levels that determine Normal IOP (between 11 and 21 mmHg [23]), it is possible to estimate the percent of fibers recruited for each tissue on the right-hand plot. The same levels of recruitment can then be noted on the left-hand plot and used to estimate the normal local stretch levels that would be required to produce the same fraction of recruited fibers (green dashed lines and arrows). Following this approach leads to an estimate that in normal IOPs PPS local stretch ranges about 4% (a slightly tighter range is estimated for the LC). These stretch levels are fairly within the order of magnitude of single-digit stretch levels predicted by many computational models [17, 27, 116] and estimated from experiments [11, 117, 118]. Note that this comparison is of the range of stretch for a range of normal IOPs. Many computational models, instead, compute stretch from a state of no pressure (0 mmHg) and a given level of normal or elevated IOP. [27] Those levels of stretch are larger, in large part due to the larger relative stretch levels at low IOPs, where the fibers are wavier and the tissues are more compliant. Whereas this process of early recruitment is clearly discernible for both PPS and LC in this study (region labeled “Initial recruitment”), it is not visible on the curve from the Jan et al. work. This is largely because in this study we were able to track more stretch levels than were possible when using population-based comparisons. In addition, there may be pre-stress/strain at 0 mmHg, which, if ignored, may lead to underestimating the strain/stress in the PPS at higher IOPs. [119, 120]